Asymptotic analysis for criticality assessment of defects in mechanical structures

Eduard Marenic, Delphine Brancherie, Marc Bonnet

▶ To cite this version:

HAL Id: hal-01922597
https://hal.archives-ouvertes.fr/hal-01922597

Submitted on 14 Nov 2018

Asymptotic analysis for criticality assessment of defects in mechanical structures

E. Marenić[1], D. Brancherie[2], M. Bonnet[3]

[1] *Institut Clément Ader (ICA), Université de Toulouse, UMR CNRS 5312-INSA, Toulouse, eduard.marenic@insa-toulouse.fr*
[2] *Laboratoire Roberval, Université de Compiegne, delphine.brancherie@utc.fr*
[3] *POems, ENSTA, Palaiseau, mbonnet@ensta.fr*

Abstract — The presented work is a step towards designing a numerical strategy capable of assessing the nocivity of a small defect in terms of its size and position in the structure with low computational cost, using only a mesh of the defect-free reference structure. The proposed strategy would allow to assess the criticality of defects by introducing trial micro-defects with varying positions, sizes and mechanical properties. The main focus of the this work is to present two computational scenarios allowing to efficiently evaluate criticality considering the effect of either a fixed flaw on a region of interest or varying flaws on a fixed evaluation point.
Key words — defect, asymptotic analysis, elastic moment tensor.

1 Introduction

The role played by defects in the initiation and development of rupture is crucial and has to be taken into account in order to realistically describe the behavior till complete failure. The difficulties in that context revolve around (i) the fact that the defect length scale is much smaller than the structure length scale, and (ii) the random nature of their position and size. Even in a purely deterministic approach, taking those defects into consideration by standard models imposes to resort to geometrical discretisations at the defect scale, leading to very costly computations and hindering parametric studies in terms of defect location and characteristics.

Our current goal is to design an efficient two-scale numerical strategy which can accurately predict the perturbation in terms of stress caused by an inhomogeneity in elastic (background) material. To make it computationally efficient, the analysis uses only a mesh for the defect-free structure, i.e. the mesh size does not depend on the (small) defect scale. The latter is instead taken into account by means of a multiscale asymptotic expansion (see e.g. [1, 2]), in which the concept of *elastic moment tensor* (EMT) [3, 4] plays an important role. After this introduction we proceed by problem definition in Sec. 2, and discuss the small-inhomogeneity solution asymptotics in Sec. 3 focusing on the outer expansion, and Green's tensor and EMT definition. The performance of the proposed approach is shown on numerical examples (Sec. 4). Conclusions and perspectives are given in the last section. This work is a continuation of [5], its main new contribution being the two alternative computational scenarios discussed in Sec. 3 and their numerical realisation.

2 Problem definition

We consider a linearly elastic body occupying a smooth bounded domain $\Omega \subset \mathbb{R}^d$ (with $d = 2$ or 3 is the spatial dimensionality), whose boundary Γ is partitioned as $\Gamma = \Gamma_D \cup \Gamma_N$; where Γ_D and Γ_N, respectively, support a prescribed traction $\bar{\mathbf{t}}$ and a prescribed displacement $\bar{\mathbf{u}}$, while a body force density $\mathbf{f}$ is applied in Ω. Based on this fixed geometrical and loading configuration, we consider two domains, namely (i) a reference solid characterized by a given elasticity tensor $\mathcal{C}$, which defines the background solution, and (ii) a perturbed solid Ω_a corresponding to Ω where a small inhomogeneity B_a of size a and elasticity tensor $\mathcal{C}^\star$ is introduced at point $\mathbf{z}$. As mentioned in the introduction, the aim of this work is to formulate a computational approach allowing to treat case (ii) as a perturbation of the background solution (i), in
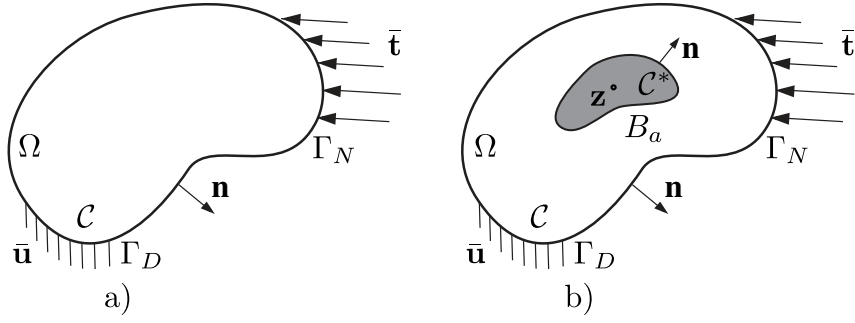
Figure 1: Reference a) and perturbed b) solids. The inhomogeneity B_a located at $\mathbf{z}$ is the shaded subdomain in b).

particular avoiding any meshing at the small inhomogeneity scale. We further seek to apply known results of the asymptotic expansion of the displacement perturbation with respect to the small characteristic size a of the inhomogeneity to case (ii).

2.1 Background problem (case (i))

The background solution in terms of displacement field $\mathbf{u}$ arising in the reference solid Ω with elasticity tensor $\mathcal{C}$ (Fig. 1a) due to prescribed loading $(\mathbf{f}, \bar{\mathbf{t}}, \bar{\mathbf{u}})$, corresponding to case (i) above, solves the problem

$$\mathrm{div}(\mathcal{C} : \varepsilon[\mathbf{u}]) + \mathbf{f} = \mathbf{0} \text{ in } \Omega, \quad \mathbf{t}[\mathbf{u}] = \bar{\mathbf{t}} \text{ on } \Gamma_N, \quad \mathbf{u} = \bar{\mathbf{u}} \text{ on } \Gamma_D, \tag{1}$$

where the linearized strain tensor $\varepsilon[\mathbf{w}]$ and the traction vector $\mathbf{t}[\mathbf{w}]$ associated with a given displacement $\mathbf{w}$ are given by

$$\text{(a) } \varepsilon[\mathbf{w}] = (\nabla \mathbf{w} + \nabla^T \mathbf{w})/2, \quad \text{(b) } \mathbf{t}[\mathbf{w}] = (\mathcal{C} : \varepsilon[\mathbf{w}]) \cdot \mathbf{n}, \tag{2}$$

with $\mathbf{n}$ denoting the unit outward normal to Γ. In (2b) and hereinafter, symbols '·' and ':' denote single and double inner products.

2.2 Transmission problem for a small inhomogeneity (case (ii))

The elastic body Ω_a occupies the same domain Ω but now contains a small defect, in the form of an inhomogeneity located at $\mathbf{z} \in \Omega$, embedded in the background material (Fig. 1b). The inhomogeneity occupies the domain $B_a := \mathbf{z} + a\mathcal{B}$, where the smooth fixed domain $\mathcal{B} \subset \mathbb{R}^d$ centered at the origin defines the defect shape, and has elastic properties described by the tensor $\mathcal{C}^\star$. The elastic properties of the whole perturbed solid are therefore defined as

$$\mathcal{C}_a := \mathcal{C}(1 - \chi_{B_a}) + \mathcal{C}^\star \chi_{B_a}, \tag{3}$$

where χ_D is the characteristic function of a domain D. For later reference, we also introduce the elasticity tensor perturbation

$$\Delta\mathcal{C} := \mathcal{C}^\star - \mathcal{C}. \tag{4}$$

The displacement field $\mathbf{u}_a$ arising in the solid containing the small inhomogeneity B_a due to the same prescribed loading $(\mathbf{f}, \bar{\mathbf{t}}, \bar{\mathbf{u}})$, solves the transmission problem

$$\mathrm{div}(\mathcal{C}_a : \varepsilon[\mathbf{u}_a]) + \mathbf{f} = \mathbf{0} \text{ in } B_a \cup (\Omega \setminus \overline{B_a}), \quad \mathbf{t}[\mathbf{u}_a] = \bar{\mathbf{t}} \text{ on } \Gamma_N, \quad \mathbf{u}_a = \bar{\mathbf{u}} \text{ on } \Gamma_D,$$
$$\mathbf{u}_a|_- = \mathbf{u}_a|_+ \quad \text{and} \quad \mathbf{t}^\star[\mathbf{u}_a]|_- = \mathbf{t}[\mathbf{u}_a]|_+ \quad \text{on } \partial B_a, \tag{5}$$

where the traction operator $\mathbf{t}^\star$ is defined by (2b) with $\mathcal{C}$ replaced by $\mathcal{C}^\star$ and the $\pm$ subscripts indicate traces from inside B_a and outside of B_a, respectively.

3 Small-inhomogeneity solution asymptotics

Let the displacement perturbation $\mathbf{v}_a := \mathbf{u}_a - \mathbf{u}$ be given as the difference of the total and unperturbed displacement, where $\mathbf{u}_a$ and $\mathbf{u}$ solve problems (5) and (1), respectively corresponding to the perturbed

and background configurations. An asymptotic analysis of $\mathbf{v}_a$ with respect to the characteristic defect size a provides two distinct expansions, namely inner and outer expansions [?]. Those expansions focus on two distinct scales: (a) the structure scale, where points are described using "ordinary" coordinates $\mathbf{x} \in \Omega$, and (b) the defect scale corresponding to the characteristic length a of the inhomogeneity, with rescaled coordinates $\bar{\mathbf{x}} := (\mathbf{x} - \mathbf{z})/a$. This description is directly related to the slow and fast variables used in [1, 2].

In this work we focus on the outer expansion given by [4, Thm. 11.4]

$$\mathbf{v}_a(\mathbf{x}) = -\nabla_{(1)}\boldsymbol{G}(\mathbf{z},\mathbf{x}) : \mathcal{A}(\mathcal{B}, \mathcal{C}, \Delta\mathcal{C}) : \nabla\mathbf{u}(\mathbf{z})a^d + o(a^d), \qquad \mathbf{x} \neq \mathbf{z}. \tag{6}$$

More precisely we focus on the computation of the *asymptotic correction*, i.e., the leading contribution to the outer approximation (6) given as

$$\widetilde{\mathbf{v}}_a(\mathbf{x}) := -\nabla_{(1)}\boldsymbol{G}(\mathbf{z},\mathbf{x}) : \mathcal{A}(\mathcal{B}, \mathcal{C}, \Delta\mathcal{C}) : \nabla\mathbf{u}(\mathbf{z})a^d. \tag{7}$$

In the above equations $\boldsymbol{G}$ is the elastostatic Green's tensor, $\nabla_{(1)}\boldsymbol{G}$ denotes the gradient with respect to the first argument of the two-variable function $\boldsymbol{G}$, and $\mathcal{A}$ is the elastic moment tensor (EMT) associated with the inhomogeneity (Sec. 3.1). Expansion (6) is expressed in terms of the slow coordinates $\mathbf{x}$ and is valid at any finite (independent of a) distance from the inhomogeneity, i.e. at the structure scale. The main ingredients of (7) are (i) the gradient of the background solution at the inhomogeneity location $\nabla\mathbf{u}(\mathbf{z})$ (or, equivalently, its strain or stress at that point), (ii) the gradient of the Green's tensor $\boldsymbol{G}$, and (iii) the elastic moment tensor (EMT) $\mathcal{A}$. In the context of the proposed computational procedure (i) is given by a FEM solution of the background problem (1). Thus, we focus further on the definition and numerical evaluation of $\mathcal{A}$ and $\nabla_{(1)}\boldsymbol{G}(\mathbf{z},\mathbf{x})$ considering two scenarios of criticality assessment, namely
(a) fixed inclusion location $\mathbf{z}$ and varying evaluation point $\mathbf{x}$, or
(b) fixed evaluation point $\mathbf{x}$ and varying inclusion location $\mathbf{z}$.
The outer expansion given by (6) assumes a single defect, but can be extended, by additive superposition, to a finite number of defects whose locations $\mathbf{z}_i$ are fixed (i.e. are independent of a), as coupling between defects occurs only at higher orders.

3.1 Elastic moment tensor

The EMT $\mathcal{A}$ associated with an inhomogeneity of shape $\mathcal{B}$ and stiffness $\mathcal{C}^\star$ embedded in a background medium of stiffness $\mathcal{C}$ is defined by

$$\mathcal{A} : \boldsymbol{E} = \int_{\mathcal{B}} \Delta\mathcal{C} : \nabla\mathbf{u}_{\mathcal{B}}[\boldsymbol{E}]\,\mathrm{d}V, \quad \forall \boldsymbol{E} \in \mathbb{R}^{d \times d}_{\text{sym}}, \tag{8}$$

where $\mathbf{u}_{\mathcal{B}}[\boldsymbol{E}]$ solves the free space transmission problem i.e. the auxiliary problem of a perfectly bonded inhomogeneity $\mathcal{B}$ embedded in an infinite elastic medium and subjected to the constant remote stress $\mathcal{C} : \boldsymbol{E}$ for given $\boldsymbol{E} \in \mathbb{R}^{d \times d}_{\text{sym}}$. Such solutions are known analytically for simple inhomogeneity shapes [6], in terms of the solution to the famous Eshelby inclusion problem [7]. The EMT carries important microstructural information, as it depends on the material properties $\mathcal{C}, \mathcal{C}^\star$ and, through $\mathcal{B}$, on the inhomogeneity shape and orientation.

We note that for ellipsoidal inclusion $\mathcal{B}$, $\nabla\mathbf{u}_{\mathcal{B}}[\boldsymbol{E}]$ is constant inside $\mathcal{B}$ [7, 6], allowing $\mathcal{A}$ to be expressed in closed form [8, 3]:
$$\mathcal{A} = |\mathcal{B}|\mathcal{C} : (\mathcal{C} + \Delta\mathcal{C} : \mathcal{S})^{-1} : \Delta\mathcal{C}, \tag{9}$$

where $\mathcal{S} = \mathcal{S}(\mathcal{B}, \mathcal{C})$ denotes the (fourth-order) Eshelby tensor of the normalized inclusion $\mathcal{B}$. The evaluation of $\mathcal{A}$ then essentially rests on that of $\mathcal{S}$. In this work we will treat the isotropic case ($\mathcal{C}$ isotropic), and we are going to benefit from the fact that $\mathcal{S}$ can be evaluated analytically.

3.2 Elastostatic Green's tensor and computational scenarios

The elastostatic Green's tensor is defined as $\boldsymbol{G}(\boldsymbol{\xi},\mathbf{x}) = \mathbf{e}_k \otimes \boldsymbol{G}^k(\boldsymbol{\xi},\mathbf{x})$, where the displacement field $\boldsymbol{G}^k(\boldsymbol{\xi},\mathbf{x})$ is the response at $\boldsymbol{\xi} \in \Omega$ of the background body subjected to (i) a unit point force applied

at $\mathbf{x} \in \Omega$ along the coordinate direction $\mathbf{e}_k$ and (ii) homogeneous boundary conditions, i.e.

$$\text{div}(\mathcal{C} : \varepsilon[\boldsymbol{G}^k(\cdot,\mathbf{x})]) + \delta(\cdot - \mathbf{x})\mathbf{e}_k = \mathbf{0} \qquad \text{in } \Omega,$$
$$\mathbf{t}[\boldsymbol{G}^k(\cdot,\mathbf{x})] = \mathbf{0} \qquad \text{on } \Gamma_N \qquad (1 \le k \le d) \qquad (10)$$
$$\boldsymbol{G}^k(\cdot,\mathbf{x}) = \mathbf{0} \qquad \text{on } \Gamma_D,$$

where δ denotes the unit Dirac mass at the coordinate origin. We introduce next the following additive decomposition of $\boldsymbol{G}$:

$$\boldsymbol{G}(\cdot,\mathbf{x}) = \boldsymbol{G}_\infty(\cdot - \mathbf{x}) + \boldsymbol{G}_c(\cdot,\mathbf{x}), \qquad (11)$$

where $\boldsymbol{G}_\infty$ is the (singular) full-space Green's tensor (also called fundamental tensor), while the complementary (non-singular) correction $\boldsymbol{G}_c$ allows $\boldsymbol{G}$ to satisfy the homogeneous boundary conditions resulting from Ω being bounded. Decomposition (11) allows to take advantage of the fact that the fundamental tensor $\boldsymbol{G}_\infty = \mathbf{e}_k \otimes \boldsymbol{G}_\infty^k$ is known analytically.

Thus, evaluation of $\boldsymbol{G}$ and its gradients only resorts to evaluation of $\boldsymbol{G}_c$ which, by virtue of problem (10) (linear) and decomposition (11), solves the following elastostatic boundary-value problem (BVP) with regular boundary data and vanishing zero body force density:

$$\text{div}(\mathcal{C} : \varepsilon[\boldsymbol{G}_c^k(\cdot,\mathbf{x})]) = \mathbf{0} \qquad \text{in } \Omega,$$
$$\boldsymbol{G}_c^k(\cdot,\mathbf{x}) = -\boldsymbol{G}_\infty^k(\cdot - \mathbf{x}) \qquad \text{on } \Gamma_D, \qquad (12)$$
$$\mathbf{t}[\boldsymbol{G}_c^k(\cdot,\mathbf{x})] = -\mathbf{t}[\boldsymbol{G}_\infty^k(\cdot - \mathbf{x})] \qquad \text{on } \Gamma_N.$$

where $\boldsymbol{G}_\infty^k$ and its derivatives on Γ are known analytically in closed form.

3.3   Two computational scenarios

To evaluate $\nabla_{(1)}\boldsymbol{G}(\mathbf{z},\mathbf{x})$ used in the asymptotic correction (7), it seems natural to solve numerically the BVPs (12) for $\boldsymbol{G}_c^k$ ($1 \le k \le d$) and then compute $\nabla_{(1)}\boldsymbol{G}(\mathbf{z},\mathbf{x}) = \nabla\boldsymbol{G}_\infty(\mathbf{z} - \mathbf{x}) + \nabla_{(1)}\boldsymbol{G}_c(\mathbf{z},\mathbf{x})$. However, while $\nabla\boldsymbol{G}_\infty$ is known analytically, $\nabla\boldsymbol{G}_c$ must in general be evaluated via numerical differentiation of the computed solution for $\boldsymbol{G}_c$, a step which is likely to entail loss of accuracy. Moreover, solving (12) for given $\mathbf{x}$ allows to evaluate $\widetilde{\mathbf{v}}_a$ via (7) for a fixed evaluation point $\mathbf{x}$ and varying inhomogeneity locations $\mathbf{z}$, i.e. is convenient for scenario (b) but incurs significant computational cost for scenario (a). We therefore propose two distinct strategies for the evaluation of $\nabla_{(1)}\boldsymbol{G}$, depending on whether scenario (a) or (b) is to be considered.

Scenario (a): fixed flaw location and varying evaluation point.   To avoid solving problem (12) for each evaluation point $\mathbf{x}$, which would cause significant computational cost for the scenario of a fixed flaw, we propose an alternative approach which consists in finding a governing elasticity problem for $\nabla_{(1)}\boldsymbol{G}(\mathbf{z},\cdot)$ with $\mathbf{z}$ fixed. We begin by using the symmetry relationship $\boldsymbol{G}(\mathbf{z},\mathbf{x}) = \boldsymbol{G}^T(\mathbf{x},\mathbf{z})$ in (7), so as to swap the roles of $\mathbf{x}$ and $\mathbf{z}$, to obtain (in component form)

$$\begin{aligned}
[\widetilde{v}_a]_k(\mathbf{x}) &= -\partial_{(1)j}G_i^k(\mathbf{z},\mathbf{x})\mathcal{A}_{ijmn}u_{m,n}(\mathbf{z})a^d \\
&= -\partial_{(2)j}G_k^i(\mathbf{x},\mathbf{z})\mathcal{A}_{ijmn}u_{m,n}(\mathbf{z})a^d
\end{aligned} \qquad (13)$$

with notations $\partial_{(1)j}$ and $\partial_{(2)j}$, respectively, indicating partial differentiation with respect to the j-th coordinate of the first and second argument of $\boldsymbol{G}$. Now, decomposition (11) implies

$$G_k^i(\cdot,\mathbf{z}) = [G_\infty^i]_k(\cdot - \mathbf{z}) + [G_c^i]_k(\cdot,\mathbf{z}), \qquad (14)$$

where $\boldsymbol{G}_c^i(\cdot,\mathbf{z})$ is governed by problem (12) with $\mathbf{x}$ replaced by $\mathbf{z}$ and k by i. Moreover, $\nabla_{(2)}\boldsymbol{G}_c$ may be defined by simply differentiating the BVP (12) with respect to the second argument of $\boldsymbol{G}_c$, which acts in (12) as a parameter, and solving the resulting derivative BVP for $\nabla_{(2)}\boldsymbol{G}_c$. Accordingly, each displacement field $\boldsymbol{H}_j^i(\cdot,\mathbf{z}) := \partial_{(2)j}\boldsymbol{G}_c^i(\cdot,\mathbf{z})$ ($1 \le i,j \le d$) solves the BVP

$$\text{div}(\mathcal{C} : \varepsilon[\boldsymbol{H}_j^i(\cdot,\mathbf{z})]) = \mathbf{0} \qquad \text{in } \Omega,$$
$$\boldsymbol{H}_j^i(\cdot,\mathbf{z}) = \partial_{(1)j}\boldsymbol{G}_\infty^i(\cdot,\mathbf{z}) \qquad \text{on } \Gamma_D, \qquad (15)$$
$$\mathbf{t}[\boldsymbol{H}_j^i(\cdot,\mathbf{z})] = \mathbf{t}[\partial_{(1)j}\boldsymbol{G}_\infty^i(\cdot,\mathbf{z})] \qquad \text{on } \Gamma_N.$$

4

Then, the asymptotic correction $\widetilde{\mathbf{v}}_a$ can be evaluated using

$$\widetilde{\mathbf{v}}_a(\mathbf{x}) = \widetilde{\mathbf{v}}_{a,\infty}(\mathbf{x}) + \widetilde{\mathbf{v}}_{a,c}(\mathbf{x}) =: \left(\partial_{(1)j}G_\infty^i(\mathbf{x}-\mathbf{z}) - H_j^i(\mathbf{x},\mathbf{z})\right)\mathcal{A}_{ijmn}u_{m,n}(\mathbf{z})a^d \qquad (16)$$

(having introduced in (13) the Green's tensor decomposition (14), and using $\nabla G_\infty(\boldsymbol{\xi}-\mathbf{x}) = -\nabla G_\infty(\mathbf{x}-\boldsymbol{\xi})$ for G_∞). Due to the symmetry of the EMT, the evaluation of the above expression entails numerically solving $d(d+1)/2$ problems (15), which are *set on the unperturbed (defect-free) configuration*.

Scenario (b): varying flaw location and fixed evaluation point. For this situation, it seems impossible to derive a problem similar to (15) whose unknown is $\partial_{(1)j}G_i^k(\cdot,\mathbf{x})$ or $\partial_{(2)j}G_k^i(\mathbf{x},\cdot)$, with $\mathbf{x}$ fixed, because the partial derivative $\partial_{(1)j}$ or $\partial_{(2)j}$ now acts on the field point rather than the source point. Consequently:

  (i) For computing displacement corrections of the form (13), one may solve problems (12) and differentiate the resulting FE solution.

 (ii) For computing strain or stress corrections, requiring derivatives of (13), one notes that

$$\partial_\ell[\widetilde{v}_a]_k(\mathbf{x}) = -\partial_{(2)\ell}\partial_{(1)j}G_i^k(\mathbf{z},\mathbf{x})\mathcal{A}_{ijmn}u_{m,n}(\mathbf{z})a^d$$
$$= -\partial_{(1)j}[H_\ell^k(\mathbf{z},\mathbf{x})]_i\mathcal{A}_{ijmn}u_{m,n}(\mathbf{z})a^d$$

Such evaluations may therefore be performed by solving problem (15) with $\mathbf{z} = \mathbf{x}$ (i.e. the source point for problem (15) set equal to the fixed evaluation point $\mathbf{x}$), and then differentiating the resulting numerical solution for $H_\ell^k(\cdot,\mathbf{x})$.

4 Numerical examples

The proposed approach is now illustrated on the example of the bending of a thick beam featuring a single small elliptic inhomogeneity (Fig. 2). This example concerns the bending of a simply supported beam
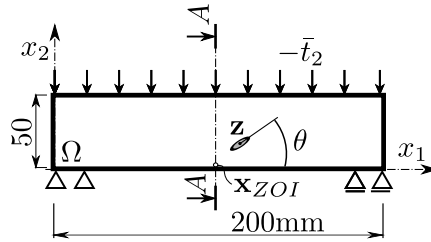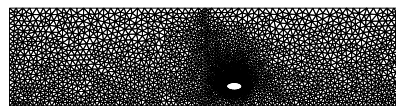

Figure 2: Geometry and boundary conditions of the thick beam under bending load.

(of size 200×50 mm^2) loaded on its top side with uniformly distributed normal load $\bar{t}_2 = -30$ MPa. The material properties are given as $E = 380000$ MPa, and $\nu = 0.18$. The inhomogeneity is taken as an elliptic hole located at $\mathbf{z} = (115,10)$, whose major semiaxis a_1 has an inclination angle θ relatively to the x_1 direction (see Fig. 2b). The defect size is defined in terms of the semiaxes $a_1 = 4$, $a_2 = 2$, except where stated differently. To compare the "brute force" solution $\mathbf{u}_a^h$ of problem (5) which considers a
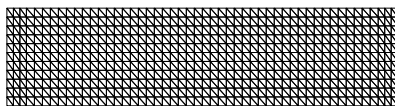
(a) Reference solid, coarse mesh M_H (289 nodes)   **(b)** Perturbed solid, fine mesh M_h (5062 nodes)

Figure 3: Finite element meshes.

discretisation of domain Ω_a to its asymptotic approximation $\widetilde{\mathbf{u}}_a^H$, we introduce the fine mesh M_h (Fig.3b) modelling the inhomogeneity (i.e. entailing mesh refinement at the defect scale in a neighbourhood of B_a). All finite element solutions discussed in this section (such as $\widetilde{\mathbf{u}}_a^H$ or $\mathbf{u}_a^h$) are labelled with the characteristic element size H or h (with $h \leq H$) of the mesh used for the computation. The numerical results to follow were obtained by means of the code FEAP [9], using meshes made of three-node triangulars elements with continuous piecewise-linear displacement interpolation.

5

4.1 Scenario (a): fixed flaw location and varying evaluation point

For the scenario (a) we will discuss the criticality of the inhomogeneity in terms of the stress perturbation, which is usually taken as the quantity of interest for the design of structural components. Accordingly, we present the comparison of the computed asymptotic correction $\tilde{\mathbf{v}}_a^H$ versus the reference solution $\mathbf{v}_a^h$ (on the fine mesh M_h).

Remark 1. Computing $\tilde{\mathbf{v}}_a^H$ entailed four FE solutions on M_H (one for the background problem (1), three for problems (15) with $1 \leq i \leq j \leq 2$), each requiring about .15s, while obtaining comparison solution $\mathbf{u}_a^h$ on the fine mesh M_h required about 6.6s. While these CPU timings are all very moderate, our approach applied to this example performs about ten times faster than straightforward analyses on meshes involving the defect scale, and this relative advantage is expected to increase for similar analyses on three-dimensional configurations.

Results in terms of evaluation of the asymptotic approximation $\tilde{\sigma}_a^H := C : \varepsilon[\tilde{\mathbf{v}}_a^H]$ of the (linear elastic) stress perturbation induced by the defect, and its comparison with the reference stress perturbation $\sigma_a^h := C_a : \varepsilon[\mathbf{v}_a^h]$ are presented in Fig. 4 (for component σ_{11}). We can note that the asymptotic stress perturbation $\tilde{\sigma}_a^H$, computed on M^H, compares well with its reference counterpart σ_a^h computed on M^h (note that the scale and colormap are chosen so as to emphasize the far field character of the outer expansion, based on (6)). We also note that in the close vicinity of the inhomogenity (see zoom on Fig. 4) the refer-
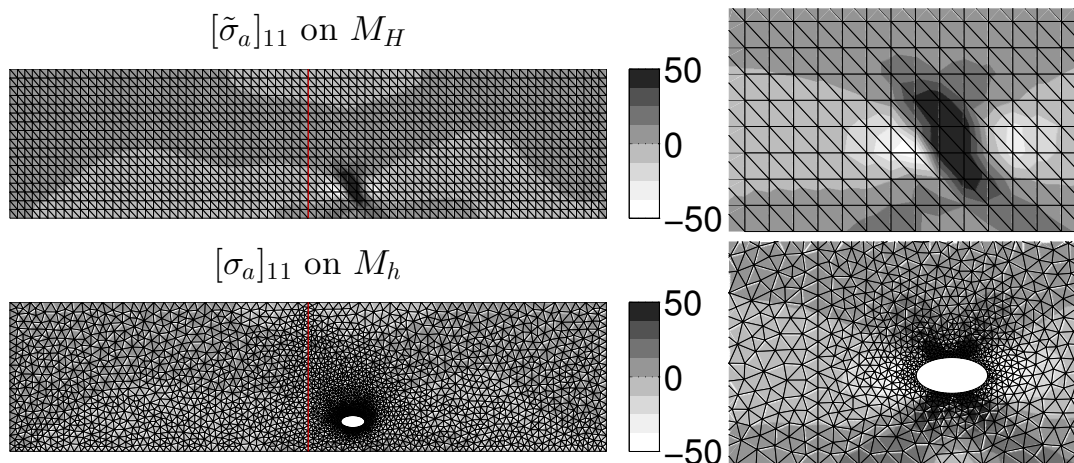

Figure 4: Contour plots of the asymptotic approximation $\tilde{\sigma}_a^H$ of the stress perturbation (upper plots) and the reference perturbation σ_a^h (lower plots). The plots on the right are zooms showing both fields in the vicinity of $\mathbf{z}$. The elliptic hole is located at $\mathbf{z} = (115, 10)$, and its inclination is $\theta = 0$.

ential solution is for sure a mixture of inner and outer expansion rather then pure outer. Having verified our approach we proceed with criticality assessment by the evaluation of $\tilde{\sigma}_a^H$ for various inhomogeneity orientations and shapes. The definition of the criticality naturally depends on the application. For the perturbation in terms of stress (usual choice in engineering) the criticality would usually be related to the ratio of perturbation with respect to the unperturbed stress. For the criticality study we are going to benefit from the developed method and its main advantage. Namely, using the presented computational procedure (denoted as scenario (a)) for the given background and inhomogeneity properties (both being isotropic) and position $\mathbf{z}$, we can compute stress perturbation distribution ($\forall \mathbf{x} \in \Omega \setminus B$) for various inhomogeneity orientations and shapes without any additional computational cost. More precisely, searching for the critical defect then boils down to simple *evaluation of EMT* (analytical expression) for different inhomogeneity orientations θ and shapes defined here through a_1 and a_2.

Thus, we obtain the evolution of the most significant in plane component of the stress perturbation distribution along the crossection $A - A$ (measured with x_2) in Figure 2. Here the inhomogeneity is taken as an elliptic hole which orientation θ and principal axes ratio a_1/a_2 are taken as denoted in the Fig. 5 It can be noted that the orientation of $\theta = 90°$ yields the highest peak in stress perturbation along the crossection (see yellow curve in Figure 5). Moreover, we can note that when changing the inhomogeneity shape, that is, increasing principal axes ratio and keeping the surface of the elliptical defect fixed, we recover the intuitive results giving that sharper elliptical defects are more critical (in terms of stress perturbation).
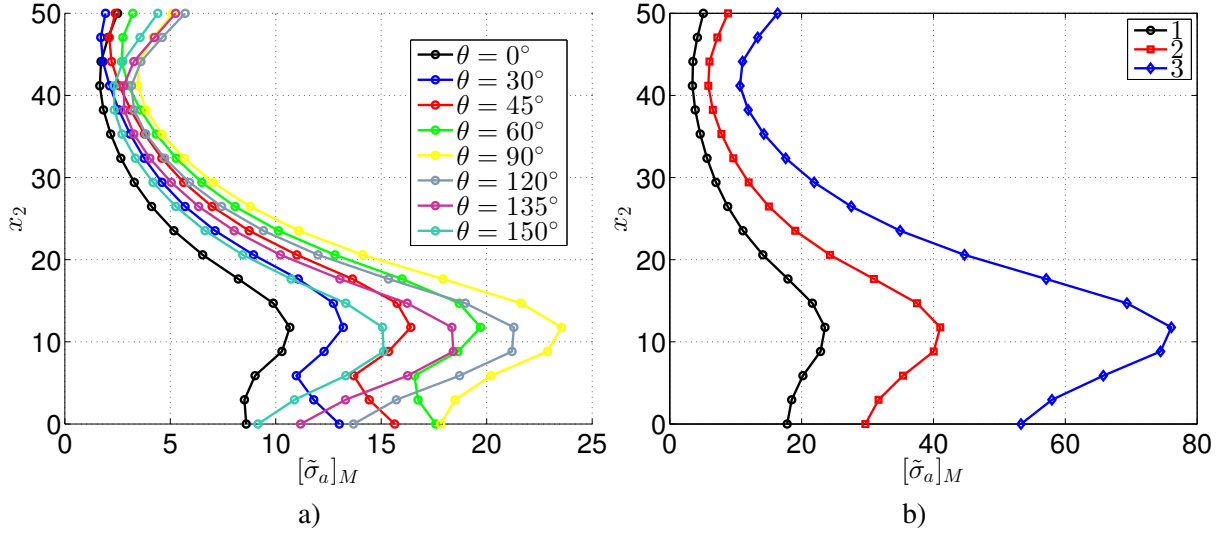
Figure 5: Distribution of the asymptotic approximation in terms of von Mises stress perturbation $[\tilde{\sigma}_a^H]_M$ along the crossection $A - A$ given as x_2. The elliptic hole is located at $\mathbf{z} = (115, 10)$. Its principal axes are rotated with respect to global coordinate system for θ (shown as parameter on a)). Following the peak perturbation from a) the angle $\theta = 90°$ is fixed on plot b) with the semiaxes ratio $(a_1/a_2) = \{(4/2), (4\sqrt{2}, \sqrt{2}), (8, 1)\}$, for the curves 1, 2 and 3, respectively.

4.2 Scenario (b): varying flaw location and fixed evaluation point

In order to complete the criticality definition and analysis introduced above, we turn to scenario (b) where the flaw (i.e. $\mathbf{z}$) varies while the evaluation point $\mathbf{x}$ is fixed, as described in Sec. 3.2. In this case, we are aiming at defining the most critical position of a defect (with respect to a given criterion) evaluated at a fixed point of interest (given as e.g. $\mathbf{x}_{ZOI}$ in Fig. 2). Remember that we solve first the BVP (15) with the source point for problem (15) set equal to the fixed evaluation point, and then differentiating the resulting numerical solution for $H_\ell^k(\cdot, \mathbf{x})$. For the scenario (b), the stress corrections are given in terms of the contour plot (the three in plane components are computed and an equivalent Mises stress is plotted), as shown in Figure 6. The interpretation of the given diagrams is the following: on the chosen point $\mathbf{z} \in \Omega$, $\mathbf{z} \neq \mathbf{x}$ from the contour plots, we read the stress correction appearing on the fixed evaluation point $\mathbf{x}$, given that the flaw is located at $\mathbf{z}$. Following the above discussion related to the criticality, we can note that for scenario (b) with fixed evaluation point and varying flaw a "criticality map" is obtained. As mentioned above, the specific application imposes the real criticality criteria. Taking for instance the stress measure (component, equivalent, ...) as criteria, the contour plot (with proper contour limits) gives directly a map of criticality, that is, the region where a chosen defect (chosen type, shape, and orientation) is critical.
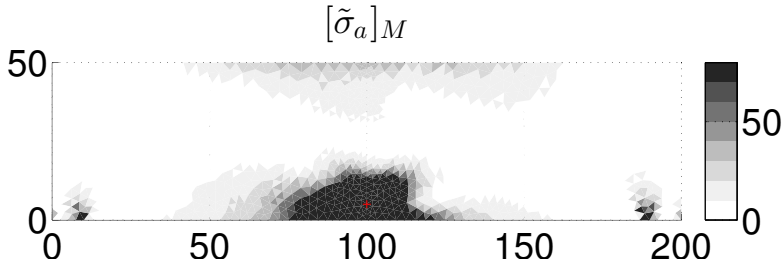
$$[\tilde{\sigma}_a]_M$$

Figure 6: Contour plot of the asymptotic approximation in terms of equivalent (Mises) stress perturbation $[\tilde{\sigma}_a]_M$ with the varying flaw $\mathbf{z}$, and fixed evaluation point $\mathbf{x} = (100, 5)$ denoted with $+$. The flaw is taken as elliptic hole with the semi-axes ratio $a_1/a_2 = 8$, and principal axes rotated with respect to global coordinate system for $\theta = 45°$. The stress perturbation is given in MPa.

Analogously as for the fixed flaw and varying evaluation point, in this approach we benefit from the main advantage of the proposed method related to the fact that the only "ingredient" carrying the information about the defect shape and properties is the EMT. Therefore, for the given background and

inhomogeneity properties (both being isotropic) and position **x**, we can compute stress perturbation in that point for various inhomogeneity positions and shapes/orientations without any additional computational cost.

5 Conclusion

A numerical strategy for predicting the perturbation caused by the local, small inhomogeneity in an elastic solid is outlined. The strategy lies on the multiscale asymptotic expansion which separates defect and structure scale through the inner and outer expansions, respectively. In this paper we focus on the structure scale which boils down to the presented computation of the outer expansion in terms of displacement correction. The biggest gain and the main feature of the presented approach is that the local inhomogeneity is not meshed, all the computations are carried out on a coarse mesh of the unperturbed domain. Key "ingredients" of the far field correction which enable us to avoid fine scale meshing are Green's and elastic moment tensors. Both of them are presented and the details about their computation is given. Special attention is given to the choice of the strategy to compute Green's tensor which further enables two interesting computational scenarios that are shown to be useful in the defect criticality assessment. A very good performance is presented on the academic example.

References

[1] Delphine Brancherie, Marc Dambrine, Grégory Vial, and Pierre Villon. Effect of surface defects on structure failure: a two-scale approach. *European Journal of Computational Mechanics*, 17(5-7):613–624, 2008.

[2] M. Dambrine and G. Vial. A multiscale correction method for local singular perturbations of the boundary. *ESAIM: Mathematical Modelling and Numerical Analysis*, 41(1):111–127, 2007.

[3] Marc Bonnet and Gabriel Delgado. The topological derivative in anisotropic elasticity. *Q J Mechanics Appl Math*, 66(4):557–586, 2013.

[4] Habib Ammari and Hyeonbae Kang. *Polarization and Moment Tensors: with Applications to Inverse Problems and Effective Medium Theory.* Springer-Verlag, New York, Applied Mathematical Sciences Series Vol. 162s, 2007.

[5] E. Marenić, D. Brancherie, and M. Bonnet. Asymptotic analysis for the multiscale modeling of defects in mechanical structures. *Actes de 12eme Colloque National en Calcul des Structures, CSMA , Giens, Var, France*, 18-22 mai 2015.

[6] Toshio Mura. *Micromechanics of Defects in Solids.* Martinus Nijhoff Publishers, 1987.

[7] J. D. Eshelby. The determination of the elastic field of an ellipsoidal inclusion and related problems. *Proc. R. Soc. Lond. A*, 241:376–396, 1957.

[8] Habib Ammari, Hyeonbae Kang, Gen Nakamura, and Kazumi Tanuma. Complete asymptotic expansions of solutions of the system of elastostatics in the presence of an inclusion of small diameter and detection of an inclusion. *Journal of elasticity and the physical science of solids*, 67(2):97–129, 2002.

[9] R. L. Taylor. FEAP - finite element analysis program, 2014.